

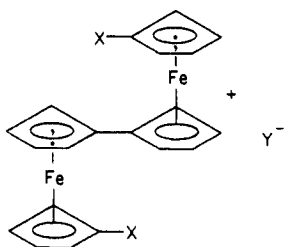
# Counterion Effects on the Intramolecular Electron-Transfer Rate of Mixed-Valence Biferrocenium Salts: Micromodulation and Phase Transitions

Teng-Yuan Dong, Takeshi Kambara,<sup>1</sup> and David N. Hendrickson\*

Contribution from the School of Chemical Sciences, University of Illinois, Urbana, Illinois 61801. Received December 2, 1985

**Abstract:** The effect of changing the counterion from  $I_3^-$  to  $I_2Br^-$ ,  $Br_2I^-$ , or  $PF_6^-$  upon the rate of *intramolecular* electron transfer in the mixed-valence biferrocenium cation is examined. Room temperature powder X-ray diffraction data are presented to show that the  $I_2Br^-$  and  $Br_2I^-$  salts are isostructural to biferrocenium triiodide. The 4.2 K X-band EPR spectrum of biferrocenium  $Br_2I^-$  is axial ( $g_{\parallel} = 3.60$  and  $g_{\perp} = 1.75$ ) and very similar to that for the  $I_3^-$  salt. However, the  $g$ -tensor anisotropy ( $g_{\parallel} = 3.23$  and  $g_{\perp} = 1.90$ ) observed for the 4.2 K EPR spectrum of biferrocenium  $I_2Br^-$  is appreciably reduced compared to that of the  $I_3^-$  and  $Br_2I^-$  salts. This probably reflects the low-symmetry environment provided by the asymmetric  $I-I-Br^-$  anion. The  $^{57}Fe$  Mössbauer characteristics of biferrocenium  $I_2Br^-$  resemble those of the  $I_3^-$  salt; however, everything is shifted to lower temperatures. The 150 K spectrum essentially consists only of two doublets (one  $Fe^{II}$  and one  $Fe^{III}$ ). A third average-valence doublet grows in with increasing temperature until at  $\sim 340$  K only this average doublet is seen. A temperature of only  $\sim 220$  K is needed to give only an average-valence doublet for the  $Br_2I^-$  salt. Thus, replacing the  $I_3^-$  by the  $Br_2I^-$  anion leads to a dramatic reduction by  $\sim 150$  deg in the temperature where the mixed-valence biferrocenium cation transfers an electron faster than the Mössbauer technique can sense. A qualitative model is developed to explain the effect of the anion replacement. The importance of the cation-cation and cation-anion interactions, as well as the intrinsic charge-oscillation barrier heights in the mixed-valence cations and anions, is discussed relative to the phase transition that is believed to be present in these compounds.

In very recent studies<sup>2-7</sup> it has been shown that the solid-state environment plays a crucial role in determining the rate of *intramolecular* electron transfer in various mixed-valence biferrocenium salts. Triiodide salts ( $Y^- = I_3^-$ ) were studied. The



triiodide salts of the mixed-valence 1',6'-dihalobiferrocenium cations ( $X = I, Br, \text{ or } Cl$ ) make up an interesting series. The  $X = I$  and  $Br$  compounds exhibit an *intramolecular* electron-transfer rate that is faster than the Mössbauer and EPR techniques can sense (i.e., faster than  $10^{10} s^{-1}$ ) from 300 K down to 4.2 K.<sup>2,5,7-9</sup> However, these two mixed-valence species do *not* have a delocalized electronic structure. That is, infrared spectra show the presence of both  $Fe^{II}$  and  $Fe^{III}$  moieties for each mixed-valence cation.<sup>2,5</sup> There is a potential-energy barrier in these  $X = I$  or  $Br$  biferrocenium salts. On the other hand, the rate of electron

transfer is less than can be sensed by the Mössbauer technique (i.e.,  $< 10^7 s^{-1}$ ) for the  $X = Cl$  analogue<sup>5,9</sup> which crystallizes with 0.5 mol of  $I_2$  in addition to the  $I_3^-$  counterion. From X-ray structural results for the  $X = I^{2,5}$  and  $Cl^5$  triiodides it has been concluded that it is the positioning of the triiodide anion relative to the mixed-valence cation that controls the rate of *intramolecular* electron transfer in the cation. For the  $X = I$  and  $Br$  compounds the  $I_3^-$  anions are symmetrically disposed relative to the two iron ions in a given mixed-valence cation. Consequently, the ground-state double-well potential-energy surface is symmetric. The two vibronic states of the mixed-valence cation,  $Fe_a^{II} Fe_b^{III}$  and  $Fe_a^{III} Fe_b^{II}$ , are at the same energy, and *intramolecular* electron transfer is relatively fast (tunneling?). The  $I_3^-$  anions in the  $X = Cl$  compound are not symmetrically disposed relative to the two iron ions in each cation. The  $Fe^{III}$  ion is on the average closer to the terminal charge-carrying iodine atoms of neighboring  $I_3^-$  anions. Thus, one vibronic state, say  $Fe_a^{II} Fe_b^{III}$ , is at appreciably lower energy than the other. As a result, the barrier for *intramolecular* electron transfer in the  $X = Cl$  cation is much larger than for the  $X = I, Br$  compounds.

Four 1',6'-dialkylbiferrocenium triiodides ( $X = CH_2CH_3, CH_2CH_2CH_3, CH_2CH_2CH_2CH_3, \text{ and } CH_2C_6H_5$ ) have also been studied.<sup>4,10</sup> These four complexes give temperature-dependent Mössbauer spectra. At temperatures less than  $\sim 200$  K, they each show two doublets, one for the  $Fe^{II}$  and the other for the  $Fe^{III}$  site. Increasing the sample temperature in each case leads to the two doublets moving together, eventually to become a single average doublet at temperatures of 275, 245, 275, and 260 K, respectively. X-ray structures have been reported at 298 and 110 K for the dipropyl compound<sup>11</sup> and at 363, 298, and 150 K for the di-*n*-butyl compound.<sup>4</sup> We suggested that the temperature dependence in electron transfer seen for these four compounds occurred as the result of the onset of motion in the solid state.<sup>4,7</sup> The motion could involve, in part, the triiodide ions interconverting between two configurations, one which can be described in a limiting form as  $I_A \cdots I_B - I_C$  and the other as  $I_A - I_B \cdots I_C$ . In each configuration

(1) On sabbatical leave from the Department of Engineering Physics, The University of Electro-Communications, Chofu, Tokyo 182, Japan.

(2) Dong, T.-Y.; Cohn, M. J.; Hendrickson, D. N.; Pierpont, C. G. *J. Am. Chem. Soc.* **1985**, *107*, 4777.

(3) Cohn, M. J.; Dong, T.-Y.; Hendrickson, D. N.; Geib, S. J.; Rheingold, A. L. *J. Chem. Soc., Chem. Commun.* **1985**, 1095.

(4) Dong, T.-Y.; Hendrickson, D. N.; Iwai, K.; Cohn, M. J.; Rheingold, A. L.; Sano, H.; Motoyama, I.; Nakashima, S. *J. Am. Chem. Soc.* **1985**, *107*, 7996.

(5) Dong, T.-Y.; Hendrickson, D. N.; Pierpont, C. G.; Moore, M. F. *J. Am. Chem. Soc.* **1986**, *108*, 963.

(6) Moore, M. F.; Wilson, S. R.; Cohn, M. J.; Dong, T.-Y.; Mueller-Westerhoff, U. T.; Hendrickson, D. N. *Inorg. Chem.* **1985**, *24*, 4559.

(7) Hendrickson, D. N.; Oh, S. M.; Dong, T.-Y.; Moore, M. F. *Comments Inorg. Chem.* **1985**, *4*, 329.

(8) Morrison, W. H., Jr.; Hendrickson, D. N. *Inorg. Chem.* **1975**, *14*, 2331.

(9) Motoyama, I.; Suto, K.; Katada, M.; Sano, M. *Chem. Lett.* **1983**, 1215.

(10) Iijima, S.; Saida, R.; Motoyama, I.; Sano, H. *Bull. Chem. Soc. Jpn.* **1981**, *54*, 1375.

(11) Konno, M.; Hyodo, S.; Iijima, S. *Bull. Chem. Soc. Jpn.* **1982**, *55*, 2327.

one I-I bond in the  $I_3^-$  anion is shorter than the other. In short, the onset of charge oscillation in the  $I_3^-$  anion directly affects the intramolecular electron transfer in the mixed-valence cation. The presence of a phase transition involving electron transfer in biferrrocenium triiodide has been established by variable-temperature heat-capacity measurements.<sup>12</sup>

Structural data for salts of trihalide ions such as  $I_3^-$ ,  $Br-I-Br^-$ , etc., emphasize two important features. First, these trihalide ions are symmetrical in some salts<sup>13</sup> and unsymmetrical in others.<sup>14</sup> It is clearly not simply a question of the size of the cation. For example, in  $[Ph_4As]I_3$  the  $I_3^-$  anions are well separated (shortest interanion I...I contact is 5.20 Å) and they are symmetrical.<sup>13a</sup> In the alkali salts of  $I_3^-$  there is a packing of the anions rather like that of  $I_2$  molecules in crystalline iodine (shortest I...I contact distance of ~4.0 Å). Although  $Cs^+$  is a large cation, the  $I_3^-$  anion in  $CsI_3$  is unsymmetrical (I-I = 2.842 (2) and 3.038 (2) Å at 113 K),<sup>13a,14a</sup> whereas, in  $KI_3 \cdot H_2O$  the  $I_3^-$  anion is symmetrical to within 0.005 Å.<sup>13c</sup> Second, the structural differences between trihalide ions have been attributed to the different environments of the terminal atoms in the crystals.

The effect of replacing  $I_3^-$  by  $Br_2I^-$  on the structure and conductivity of the conductor bis(ethylenedithio)tetrathiafulvalene (nicknamed "ET") has been noted very recently.<sup>15</sup> It was found that  $\beta$ -(ET) $_2$ ( $Br_2I$ ) possesses a higher superconducting transition temperature ( $T_C = 2.7$  K) than  $\beta$ -(ET) $_2$ ( $I_3$ ). The dibromiodate anion is linear, i.e.,  $Br-I-Br^-$ , and on the basis of ionic radii,  $Br_2I^-$  is ~7% shorter than  $I_3^-$ . The smaller size of  $Br_2I^-$  is believed to lead to a decrease in the interstack S...S distances, thereby modifying the electrical properties.

In this paper the effect of replacing the  $I_3^-$  anion of biferrrocenium triiodide by  $Br_2I^-$ ,  $BrI_2^-$ , and  $PF_6^-$  is investigated. The dramatic changes in rates of intramolecular electron transfer that result are taken as further support for the presence of phase transitions. A qualitative model is advanced which delineates the nature of cooperative intermolecular interactions in the biferrrocenium trihalide salts. The manner in which the trihalide anions micromodulate the intramolecular electron-transfer rate in the mixed-valence biferrrocenium cation is described.

## Experimental Section

**Compound Preparation.** A sample of biferrrocene was prepared according to a literature method.<sup>16</sup> A solution of 0.1 M  $HIBr_2$  was prepared by mixing 1.03 g of  $IBr$  and 0.81 mL of 50%  $HBr$  in a 50-mL volumetric flask and then diluting to the mark with methanol.<sup>17</sup> A solution of 0.1 M  $HI_2Br$  was prepared in the same fashion, using  $I_2$  instead of  $IBr$ .

Biferrrocenium dibromiodate was prepared by dissolving biferrrocene and a stoichiometric amount of *p*-benzoquinone in hexane-benzene (1:2) at 0 °C. To this solution a stoichiometric amount of 0.1 M  $HIBr_2$  methanol solution was added dropwise with rapid stirring. The resulting solid was filtered, washed with a little cold benzene, and vacuum dried. Anal. Calcd for biferrrocenium dibromiodate ( $C_{20}H_{18}Fe_2IBr_2$ ): C, 36.58; H, 2.76; Fe, 17.01. Found: C, 36.43; H, 2.60; Fe, 16.90.

Biferrrocenium bromiodiodate was prepared in the same fashion as described for the dibromiodate salt, using 0.1 M  $HI_2Br$  methanol solution instead of 0.1 M  $HIBr_2$  solution. Anal. Calcd for biferrrocenium  $I_2Br^-$  ( $C_{20}H_{18}Fe_2BrI_2$ ): C, 34.13; H, 2.58; Fe, 15.87. Found: C, 34.10; H, 2.65; Fe, 15.71.

Biferrrocenium  $PF_6^-$  was prepared by dissolving stoichiometric amounts of a biferrrocene and *p*-benzoquinone in benzene. To this solution, a 0.1 M  $HPF_6$  methanol solution was added dropwise with rapid stirring. The

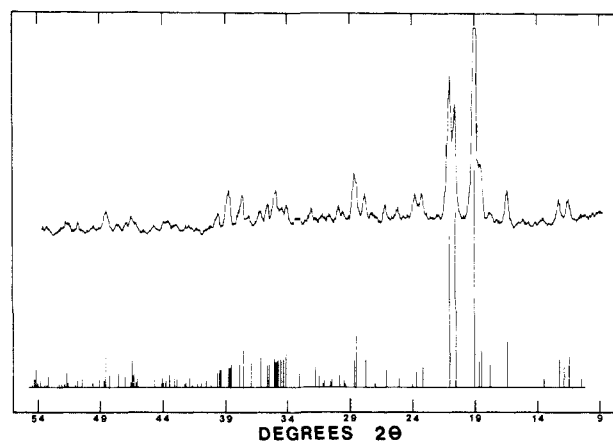


Figure 1. Room temperature powder X-ray diffraction pattern (top) for biferrrocenium triiodide. The stick diagram resulted from a computer simulation employing the unit cell parameters and atomic positional parameters from the X-ray structure.<sup>3,4</sup>

resulting solid was filtered, washed with a little benzene, and recrystallized from  $CH_2Cl_2$ . Anal. Calcd for biferrrocenium  $PF_6^-$ : C, 46.64; H, 3.52; Fe, 21.69. Found: C, 47.35; H, 3.66; Fe, 21.03.

**Physical Methods.**  $^{57}Fe$  Mössbauer measurements were made on a constant-velocity instrument which has been described previously.<sup>18</sup> Mössbauer spectra were least-squares fit to Lorentzian line shapes with a previously documented computer program.<sup>19</sup> An attempt was made to report isomer shift data relative to that of iron foil at 300 K; however, second-order Doppler effects could only be estimated due to source temperature variability (the source was located within the exchange-gas cooled cryostat). It should be noted that the isomer shifts illustrated in the figures are plotted as experimentally obtained.

Variable-temperature X-band EPR spectra of powdered samples were run on a Bruker ER200 spectrometer equipped with an Oxford Instruments temperature controller. A calibrated copper-constantan thermocouple was used to determine the sample temperature. Samples were sealed in quartz tubes which had been pumped on a glass vacuum line.

Infrared spectra were obtained with a Nicolet Model MX-5 FT spectrometer. All samples were prepared as 13-mm KBr pellets with 2-5 mg of compound mixed well with 150 mg of KBr. A Spectrim closed-cycle refrigerator (Cryogenic Technology, Inc.) was used to cool the KBr pellets to ~50 K. The temperature of the KBr pellet holder was monitored with an iron-doped gold vs. chromel thermocouple.

X-ray powder diffraction patterns were obtained on a Norelco (Phillips Electronics Co.) powder diffractometer equipped with a copper X-ray tube and a graphite monochromator. A computer program was used to simulate powder patterns.<sup>20</sup> Trial-and-error computer-simulated patterns of biferrrocenium dibromiodate were obtained by using the atom coordinates<sup>4</sup> of biferrrocenium triiodide, replacing the terminal iodine atoms with bromine atoms for trihalide anion, and then varying the unit-cell parameters. All of scattering factor constants are from the *International Tables for Crystallography*.<sup>21</sup>

## Results and Discussion

**Compound Preparation and Structure.** Mixed-valence biferrrocenium salts with  $Br_2I^-$ ,  $I_2Br^-$ , and  $PF_6^-$  counterions were prepared as microcrystalline samples by immediate precipitation following the addition of a cooled solution of  $HBr_2I$ ,  $HI_2Br$ , or  $HPF_6$ , respectively, to a cooled solution of biferrrocene and *p*-benzoquinone. A large number of attempts were made by a variety of techniques, including low-temperature recrystallizations, slow diffusion of one solvent into another, and slow evaporations, to prepare X-ray quality crystals of the  $Br_2I^-$  and  $I_2Br^-$  salts. All attempts were unsuccessful apparently due to the fact that ions such as  $Br_2I^-$  dissociate in solution to give  $IBr$  which slowly oxidatively decomposes the biferrrocene moiety. In fact, crystals which were isolated in the attempts to recrystallize the  $Br_2I^-$  salt

(12) Sorai, M.; Nishimori, A.; Dong, T.-Y.; Cohn, M. J.; Hendrickson, D. N., publication in preparation.

(13) (a) Runsink, J.; Swen-Walstra, S.; Migchelsen, T. *Acta Crystallogr.* **1972**, *B28*, 1331. (b) Soled, S.; Carpenter, G. B. *Acta Crystallogr.* **1973**, *B29*, 2556. (c) Migchelsen, T.; Vos, A. *Acta Crystallogr.* **1967**, *23*, 796. (d) General reference. (e)  $KI_3 \cdot H_2O$  structural reference.

(14) Tasman, H. A.; Boswijk, K. H. *Acta Crystallogr.* **1955**, *8*, 59.

(15) (a) Whangbo, M.-H.; Williams, J. M.; Leung, P. C. W.; Beno, M. A.; Emge, T. J.; Wang, H. H. *Inorg. Chem.* **1985**, *24*, 3500; (b) Emge, T. J.; Wang, H. H.; Beno, M. A.; Leung, P. C. W.; Firestone, M. A.; Jenkins, H. C.; Cook, J. D.; Carlson, K. D.; Williams, J. M.; Venturini, E. L.; Azevedo, L. J.; Schirber, J. E. *Inorg. Chem.* **1985**, *24*, 1738 and references therein.

(16) Rausch, M. D. *J. Org. Chem.* **1961**, *26*, 1802.

(17) Klyachko, Y. A.; Larina, O. D. *Zavod. Lab.* **1964**, *30*, 930.

(18) Cohn, M. J.; Timken, M. D.; Hendrickson, D. N. *J. Am. Chem. Soc.* **1984**, *106*, 6683.

(19) Chrisman, B. L.; Tumolillo, T. A. *Comput. Phys. Commun.* **1971**, *2*, 322.

(20) Yvon, K.; Jeitschko, W.; Parthe, E. *J. Appl. Cryst.* **1977**, *10*, 73.

(21) *International Tables for X-Ray Crystallography*; Kynoch Press: Birmingham, England, 1962; Vol. III.

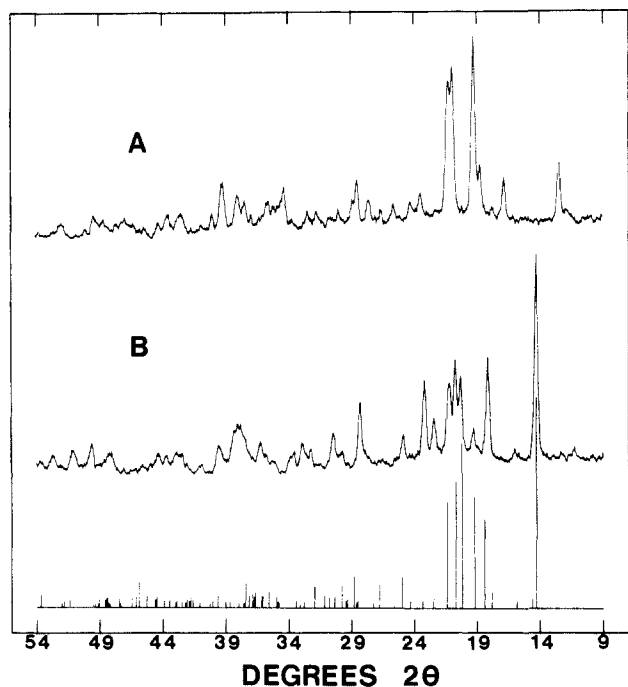


Figure 2. Room temperature powder X-ray diffraction patterns for biferrocenium  $I_2Br^-$  (A) and biferrocenium  $Br_2I^-$  (B). The stick diagram resulted from a trial-and-error simulation of the biferrocenium  $Br_2I^-$  pattern. See text for details.

were shown by a single-crystal X-ray structure to be biferrocenium tetrabromoferrate.<sup>22</sup> Obviously, the  $FeBr_4^-$  anion resulted from the decomposition of the biferrocenium ion.

The powder X-ray diffraction technique was employed to establish that the  $Br_2I^-$  and  $I_2Br^-$  biferrocenium salts have the same crystal structure as biferrocenium triiodide.<sup>3,4</sup> The room-temperature powder X-ray diffraction pattern of biferrocenium triiodide is shown in Figure 1, together with a pattern generated by a computer program utilizing the unit cell parameters and atomic positional parameters obtained from the single-crystal X-ray structure. Biferrocenium triiodide crystallizes in the  $P\bar{1}$  space group at 296 K. As can be seen in Figure 1, the computer-generated simulation does agree well with the observed powder pattern.

In Figure 2 are shown the room temperature powder X-ray diffraction patterns for the biferrocenium  $Br_2I^-$  and  $I_2Br^-$  salts. It is immediately evident that biferrocenium  $I_2Br^-$  and biferrocenium  $I_3^-$  are isostructural. Although the powder pattern for the  $Br_2I^-$  salt looks somewhat different than those obtained for the  $I_3^-$  and  $I_2Br^-$  salts, there are some similarities. Relative to  $I_3^-$  and  $I_2Br^-$  patterns, the peaks for the  $Br_2I^-$  salt seemed to be shifted to larger  $2\theta$  values, which could indicate smaller dimensions in the unit cell. In an effort to understand the origin of the differences in powder patterns, a trial-and-error approach to simulate the powder pattern of the  $Br_2I^-$  salt was tried. In this simulation approach the atomic positional parameters<sup>4</sup> of biferrocenium triiodide were maintained throughout the calculations. The unit cell parameters of biferrocenium triiodide (see Table I) were varied to generate the "best" simulated pattern shown in the Figure 2. The final unit cell parameters used to give this "best" simulation are given in Table I. The unit cell parameters result from assuming the powder pattern of the  $Br_2I^-$  salt is smaller than those for either biferrocenium  $I_3^-$  or 1',6'-di-*n*-propylbiferrocenium  $I_3^-$ , which is also of  $P\bar{1}$  symmetry. In fact, we have found that the powder pattern for biferrocenium  $Br_2I^-$  looks similar to that<sup>23</sup> for 1',6'-diethylbiferrocenium  $I_3^-$ . The packing arrangement in biferrocenium  $I_3^-$  consists of stepwise stacks of cations surrounded by stacks of anions. The above discussion, together with the fact

Table I. Unit Cell Parameters<sup>a</sup>

	biferrocenium $I_3^-$	bi- ferrocenium $Br_2I^-$	1',6'-di- <i>n</i> -propyl- biferrocenium $I_3^-$
<i>a</i> , Å	7.5779 (20)	6.5779	8.514 (8)
<i>b</i> , Å	8.4742 (14)	8.2742	8.5482 (5)
<i>c</i> , Å	9.5577 (21)	10.0577	10.9032 (13)
$\alpha$ , deg	112.619 (14)	115.488	89.546 (9)
$\beta$ , deg	104.646 (20)	105.382	115.582 (9)
$\gamma$ , deg	94.610 (19)	93.546	108.488 (7)

<sup>a</sup>Biferrocenium  $I_3^-$  crystallizes<sup>4</sup> at 296 K in the space group  $P\bar{1}$ . 1',6'-Di-*n*-propylbiferrocenium  $I_3^-$  crystallizes<sup>9</sup> at 298 K in the space group  $P\bar{1}$ . The unit cell parameters for biferrocenium  $Br_2I^-$  were obtained by simulating the X-ray powder pattern assuming that this compound also crystallizes in the  $P\bar{1}$  space group.

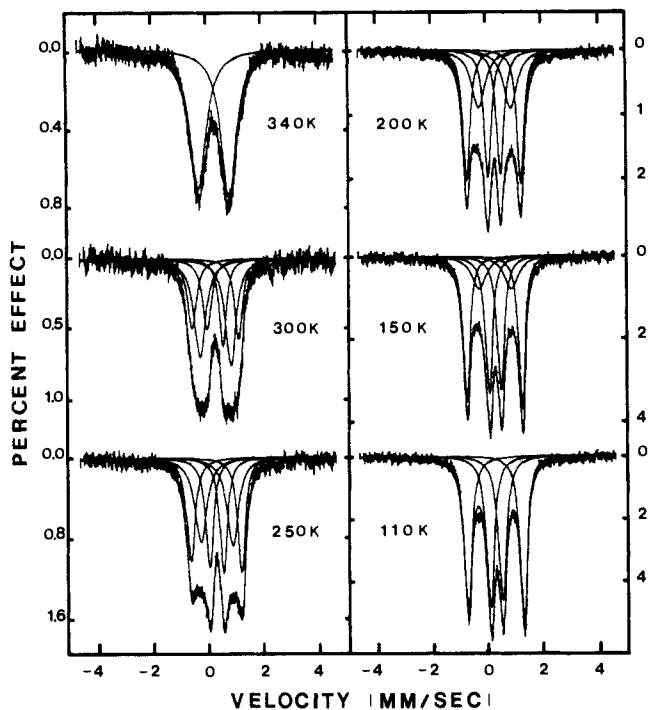


Figure 3. Variable-temperature  $^{57}Fe$  Mössbauer spectra for a microcrystalline sample of biferrocenium  $I_2Br^-$ .

that the linear  $Br-I-Br^-$  anion is only 7 to 10% shorter than  $I-I-I^-$ , makes it probable that biferrocenium  $Br_2I^-$  crystallizes in  $P\bar{1}$  and has a crystal packing arrangement not unlike the other two compounds. Very recent results<sup>24</sup> have shown that 1',6'-di-*n*-propylbiferrocenium  $I_3^-$  with its bulky substituents even has the same structure.

**$^{57}Fe$  Mössbauer Spectroscopy.** Mössbauer spectra taken for a microcrystalline sample of biferrocenium  $I_2Br^-$  are shown in Figure 3. These six spectra were least-squares fit to Lorentzian line shapes to give the parameters given in Table II. The 110 K spectrum consists of two quadrupole-split doublets, one with a quadrupole splitting ( $\Delta E_Q$ ) of 2.021 (3) mm/s and the other with  $\Delta E_Q = 0.441$  (3) mm/s. Both doublets have the same spectral area. This pattern of two doublets is what is expected for a mixed-valence biferrocene which is valence trapped on the time scale of the  $^{57}Fe$  Mössbauer experiment. In the least-squares fitting of the 150 K spectrum a third doublet with  $\Delta E_Q = 1.173$  (16) mm/s was added to get a good fit. This third doublet has the characteristics of a mixed-valence biferrocene with an intramolecular electron-transfer rate greater than  $\sim 10^7 s^{-1}$ . Increasing the temperature of biferrocenium  $I_2Br^-$  above 150 K leads to an increase in the relative intensity of this third doublet at the expense of the  $Fe^{II}$  and  $Fe^{III}$  doublets. As can be seen in Figure 3, at temperatures above  $\sim 340$  K only the third doublet can be seen. The intramolecular electron transfer is occurring at a rate faster

(22) Geib, S. J.; Rheingold, A. L.; Dong, T.-Y.; Hendrickson, D. N. *J. Organomet. Chem.*, in press.

(23) Dong, T.-Y.; Cohn, M. J.; Hendrickson, D. N., unpublished results.

(24) Pierpont, C. G.; Dong, T.-Y.; Hendrickson, D. N., unpublished results.

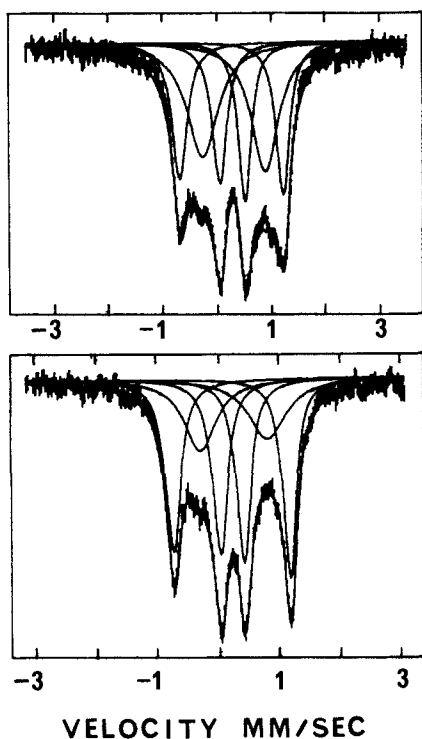


Figure 4.  $^{57}\text{Fe}$  Mössbauer spectra taken at 300 K for two different samples of biferrrocenium triiodide.

than can be sensed by the Mössbauer technique.

A comparison of the Mössbauer data reported<sup>3,4</sup> for biferrrocenium  $\text{I}_3^-$  with those for the  $\text{I}_2\text{Br}^-$  salt indicates that these two compounds have similar Mössbauer temperature dependencies; however, everything is shifted to lower temperatures for the  $\text{I}_2\text{Br}^-$  salt. As is evident in Figure 3, the  $\text{I}_2\text{Br}^-$  salt gradually converts over a large temperature range ( $\sim 200$  deg) from localized to delocalized on the Mössbauer time scale. With biferrrocenium  $\text{I}_3^-$  we have found that the range over which the spectrum changes ( $\sim 70$  deg) is smaller than that for the  $\text{I}_2\text{Br}^-$  salt and that this behavior is sample-history dependent.<sup>23</sup> For example, samples prepared by different crystallization approaches (evaporation, sudden precipitation, diffusion growth) give 300 K Mössbauer spectra with different amounts of localized and delocalized species (see Figure 4). The presence of a phase transition is indicated, which has been conclusively verified for biferrrocenium  $\text{I}_3^-$  by heat-capacity and DSC measurements.<sup>12</sup> The variability in properties of these compounds from one analytically pure sample to another is a reflection of differences in the concentration of defect structure. The presence of defect structure such as crystallographic dislocations will tend to make a phase transition occur over a larger temperature range.

An amazing change in the Mössbauer characteristics results when the  $\text{I}_3^-$  anion of biferrrocenium  $\text{I}_3^-$  is replaced by the  $\text{Br-I-Br}^-$  anion. Biferrrocenium dibromiodate is localized at temperatures below  $\sim 150$  K (see Figure 5), but increasing the temperature of the  $\text{Br}_2\text{I}^-$  salt up to 210 K gives a spectrum with but one "valence-delocalized" doublet. Mössbauer fitting parameters are given in Table II. The change from  $\text{I}_3^-$  to  $\text{Br}_2\text{I}^-$  leads to a change of  $\sim 150$  K in the temperature at which the mixed-valence biferrrocenium ion transfers electrons faster than the Mössbauer time scale. This dramatic change clearly indicates that the solid-state environment about the mixed-valence biferrrocenium cation plays a crucial role in determining the rate of *intramolecular* electron transfer in this mixed-valence cation. A model which incorporates the possible *intermolecular* interactions in these mixed-valence biferrrocenium salts is presented below.

In Figure 6 are shown variable-temperature Mössbauer spectra for a microcrystalline sample of biferrrocenium  $\text{PF}_6^-$ . The Mössbauer behavior of this  $\text{PF}_6^-$  salt is quite different from those seen for the  $\text{I}_3^-$ ,  $\text{Br}_2\text{I}^-$ , and  $\text{I}_2\text{Br}^-$  salts of the mixed-valence biferrrocenium cation. Even without a computer fitting, it is clear

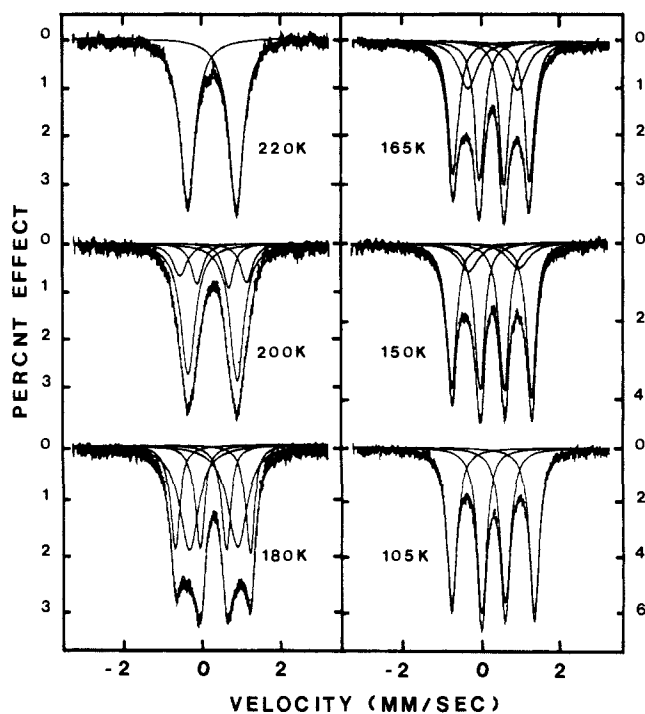


Figure 5. Variable-temperature  $^{57}\text{Fe}$  Mössbauer spectra for a microcrystalline sample of biferrrocenium  $\text{Br}_2\text{I}^-$ .

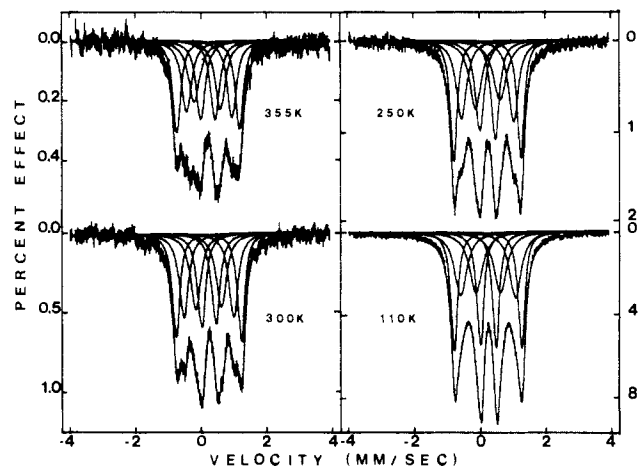


Figure 6. Variable-temperature  $^{57}\text{Fe}$  Mössbauer spectra for a microcrystalline sample of biferrrocenium  $\text{PF}_6^-$ .

from the 250 and 300 K spectra that there are at least six absorption peaks. However, it is not possible to fit these spectra by assuming that they consist of six lines that result from a superposition of a valence-localized pattern of two doublets of equal area (i.e., one  $\text{Fe}^{\text{II}}$  and one  $\text{Fe}^{\text{III}}$  doublet) and one other doublet. After trying a number of different fitting schemes, it was concluded that the spectra consist of a superposition of two valence-localized patterns, that is, eight Lorentzian line shapes where for each group of four lines the areas of each line are equal. The resulting least-squares fitting parameters are summarized in Table II. One four-line  $\text{Fe}^{\text{II}}, \text{Fe}^{\text{III}}$  valence-localized pattern does not exhibit much of a temperature dependence. For this pattern at 110 K  $\Delta E_{\text{O}}(\text{Fe}^{\text{II}})$  is 2.063 (2) mm/s and  $\Delta E_{\text{O}}(\text{Fe}^{\text{III}})$  is 0.476 (3) mm/s, whereas these values change little to become 1.926 (9) and 0.440 (15) mm/s, respectively, at 355 K. The other four-line pattern does exhibit a temperature dependence which is evident from an inspection of the spectra. For this second pattern,  $\Delta E_{\text{O}}(\text{Fe}^{\text{II}})$  varies from 1.679 (5) to 1.392 (15) mm/s and  $\Delta E_{\text{O}}(\text{Fe}^{\text{III}})$  from 0.752 (6) to 0.802 (23) mm/s as the sample temperature is varied from 110 to 355 K. For this sample of biferrrocenium  $\text{PF}_6^-$  the area ratio of the two four-line patterns was found to be close to 1:1; however, for a second microcrystalline sample we found that this ratio is appreciably different. It is likely that the four-line pattern

Table II.  $^{57}\text{Fe}$  Mössbauer Least-Squares Fitting Parameters for Mixed-Valence Biferrocenium Salts<sup>a</sup>

counterion of biferrocenium salt	T, K	$\Delta E_Q$ , mm/s	$\delta$ , mm/s	$\Gamma^b$ , mm/s	% deloc	% loc
$\text{I}_3^-$ <sup>c</sup>	300	1.901 (4)	0.473 (2)	0.298 (11); 0.256 (10)	30.4	69.6
		1.097 (17)	0.526 (9)	0.626 (86); 0.742 (94)		
		0.383 (4)	0.481 (2)	0.292 (8); 0.256 (10)		
	300	1.898 (6)	0.501 (3)	0.324 (18); 0.278 (7)	46.6	53.4
		1.147 (10)	0.548 (5)	0.680 (60); 0.602 (57)		
		0.458 (6)	0.518 (3)	0.316 (14); 0.290 (15)		
$\text{I}_2\text{Br}^-$	340	1.115 (7)	0.525 (4)	0.706 (14); 0.662 (13)	100	0
	300	1.684 (27)	0.406 (13)	0.388 (56); 0.334 (53)	47.4	52.6
		1.117 (14)	0.503 (7)	0.500 (10); 0.460 (114)		
	250	0.568 (25)	0.494 (13)	0.386 (46); 0.310 (50)	37.0	63.0
		1.836 (9)	0.496 (5)	0.362 (22); 0.326 (21)		
		1.156 (10)	0.517 (5)	0.522 (74); 0.496 (72)		
	200	0.504 (9)	0.508 (4)	0.340 (18); 0.324 (18)	30.2	69.8
		1.961 (4)	0.498 (2)	0.306 (11); 0.298 (10)		
		1.160 (11)	0.532 (5)	0.590 (64); 0.590 (63)		
	150	0.455 (4)	0.515 (2)	0.312 (9); 0.320 (9)	19.8	80.2
		2.005 (3)	0.495 (1)	0.284 (7); 0.269 (6)		
		1.173 (16)	0.550 (8)	0.622 (85); 0.620 (83)		
110	0.427 (3)	0.518 (1)	0.302 (6); 0.308 (6)	0.0	100.0	
	2.021 (3)	0.501 (1)	0.326 (4); 0.302 (4)			
		0.441 (3)	0.523 (1)	0.332 (5); 0.348 (5)		
$\text{IBr}_2^-$	260	1.196 (4)	0.514 (2)	0.450 (7); 0.438 (7)	100	0
	220	1.208 (3)	0.524 (2)	0.510 (6); 0.490 (6)	100	0
	210	1.218 (3)	0.530 (2)	0.558 (6); 0.542 (6)	100	0
	200	1.823 (39)	0.508 (19)	0.426 (52); 0.388 (53)	68.0	32.0
		1.196 (5)	0.519 (3)	0.448 (41); 0.456 (36)		
		0.654 (36)	0.560 (18)	0.376 (50); 0.526 (44)		
	190	1.820 (22)	0.525 (11)	0.414 (34); 0.378 (34)	42.6	57.4
		1.201 (7)	0.528 (4)	0.468 (75); 0.456 (71)		
		0.680 (15)	0.543 (8)	0.372 (28); 0.396 (24)		
	180	1.905 (6)	0.515 (3)	0.310 (16); 0.306 (15)	40.4	59.6
		1.205 (11)	0.541 (6)	0.620 (56); 0.630 (52)		
		0.624 (5)	0.537 (3)	0.302 (14); 0.312 (14)		
	170	1.940 (3)	0.518 (2)	0.322 (10); 0.304 (9)	21.8	78.2
		1.188 (17)	0.561 (8)	0.600 (78); 0.680 (75)		
		0.606 (3)	0.539 (2)	0.310 (7); 0.320 (8)		
150	1.992 (3)	0.521 (1)	0.348 (4); 0.324 (4)	0	100	
	0.608 (2)	0.540 (1)	0.324 (4); 0.346 (4)			
	2.071 (2)	0.524 (1)	0.330 (4); 0.298 (4)			
		0.572 (2)	0.546 (1)	0.292 (4); 0.320 (4)	0	100
$\text{PF}_6^-$ <sup>d</sup>	355	1.926 (9)	0.469 (4)	0.280 (13); 0.292 (14)		
		1.392 (15)	0.505 (8)	0.362 (26); 0.336 (20)		
		0.802 (23)	0.443 (12)	0.420 (43); 0.376 (31)		
		0.440 (15)	0.463 (7)	0.328 (22); 0.324 (24)		
	330	1.952 (7)	0.473 (4)	0.306 (12); 0.254 (9)		
		1.457 (12)	0.488 (6)	0.398 (22); 0.316 (13)		
		0.800 (13)	0.452 (6)	0.366 (22); 0.366 (20)		
		0.421 (9)	0.466 (4)	0.306 (14); 0.296 (14)		
	300	2.000 (6)	0.472 (3)	0.272 (9); 0.258 (8)		
		1.526 (9)	0.479 (4)	0.336 (13); 0.336 (13)		
		0.788 (13)	0.471 (6)	0.370 (19); 0.382 (21)		
		0.440 (9)	0.473 (4)	0.300 (13); 0.310 (14)		
	250	2.056 (3)	0.476 (2)	0.242 (5); 0.248 (5)		
		1.601 (7)	0.486 (3)	0.364 (10); 0.360 (10)		
		0.754 (14)	0.490 (7)	0.426 (20); 0.494 (23)		
		0.472 (8)	0.486 (4)	0.326 (12); 0.294 (9)		
	150	2.067 (2)	0.481 (1)	0.252 (4); 0.246 (3)		
		1.659 (5)	0.483 (2)	0.410 (8); 0.380 (7)		
		0.747 (7)	0.490 (4)	0.436 (12); 0.458 (12)		
		0.468 (4)	0.488 (2)	0.270 (5); 0.260 (4)		
	110	2.063 (2)	0.482 (1)	0.240 (3); 0.246 (3)		
1.679 (5)		0.490 (2)	0.448 (8); 0.430 (8)			
0.752 (6)		0.493 (3)	0.466 (11); 0.470 (11)			
0.476 (3)		0.490 (1)	0.250 (3); 0.244 (3)			

<sup>a</sup>The estimated standard deviations in the least-significant figures are given in parentheses. <sup>b</sup>Full width at half-height taken from the least-squares fitting program. The width for the line at more negative velocity is listed first for each doublet. <sup>c</sup>Two different samples of biferrocenium triiodide were examined. Each was prepared by slowly adding a benzene solution of  $\text{I}_2$  to a benzene solution of biferrocene over a period of 3 h. <sup>d</sup>Fitted into two sites which have 1:1 ratio.

is associated with biferrocenium cations which have an *intra*-molecular electron-transfer rate that is increasing with increasing temperature. The other four-line pattern reflects the presence of biferrocenium cations that remain valence localized on the

Mössbauer time scale perhaps because of defect structure. It is unfortunate that the considerable efforts to grow a crystal of biferrocenium  $\text{PF}_6^-$  suitable for an X-ray structure determination were unsuccessful.

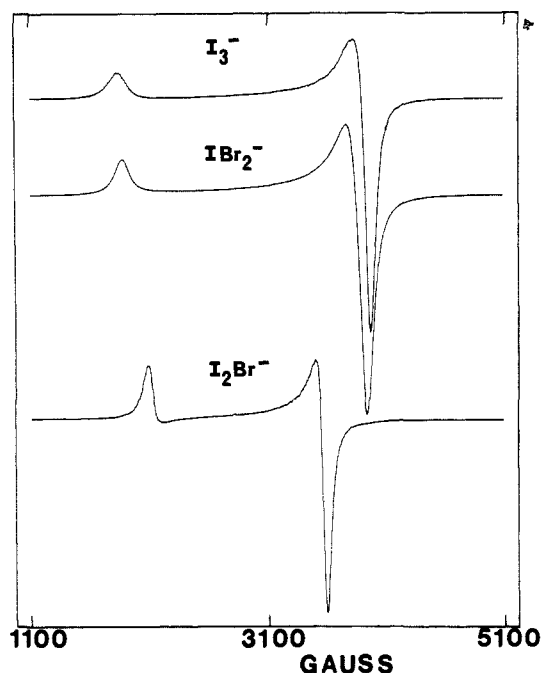


Figure 7. X-band EPR spectra for powdered samples of three biferrocenium salts at 4.2 K. The anions are indicated in the figure.

Table III. Electron Paramagnetic Resonance Data for Biferrocenium Salts<sup>a</sup>

counterion for biferrocenium salt	<i>T</i> (K)	$g_{\parallel}$	$g_{HT}^b$	$g_{\perp}$	$\Delta g^c$
$I_3^-$	4	3.66		1.73	1.93
$I_2Br^-$	3.9	3.23		1.90	1.33
$Br_2I^-$	4	3.60		1.75	1.85
	22	3.60		1.75	1.85
	60	3.57		1.76	1.81
$PF_6^-$	4	2.65	2.01	1.86	0.79
	90	2.64		2.00	
	140		2.07		

<sup>a</sup> EPR spectra were run for microcrystalline samples. <sup>b</sup>  $g_{HT}$  is calculated for the derivative-like feature which dominates the EPR spectrum at high temperatures. <sup>c</sup> This is the *g*-tensor anisotropy defined as  $\Delta g = g_{\parallel} - g_{\perp}$ .

**Electron Paramagnetic Resonance.** EPR has proven to be useful in the study of mixed-valence biferrocenes.<sup>5,8</sup> Localized  $Fe^{III}$  metallocenes generally give EPR signals only at low temperatures.<sup>25</sup> The orbital angular momentum in the ground state leads to appreciable *g*-tensor anisotropy,  $\Delta g = g_{\parallel} - g_{\perp}$ . Ferrocenium triiodide gives an axial 20 K EPR signal characterized by  $g_{\parallel} = 4.35$  and  $g_{\perp} = 1.26$  ( $\Delta g = 3.09$ ). This *g*-tensor anisotropy can be reduced by a distortion of the  $Fe^{III}$  metallocene; a trimethylene strap between the two rings of a  $Fe^{III}$  metallocene tilts the two rings relative to each other and this explains why 1,1'-trimethyleneferrocenium hexafluorophosphate has  $g_{\parallel} = 3.86$  and  $g_{\perp} = 1.81$  with  $\Delta g = 2.05$ .<sup>25</sup> Mixed-valence biferrocenes that either have delocalized electronic structures with no potential-energy barrier for electron transfer or have an intramolecular electron-transfer rate in excess of the EPR time scale empirically have been found<sup>5</sup> to have  $\Delta g$  values less than  $\sim 0.8$ . This is a reflection of considerably reduced orbital angular momentum in the ground state which results from admixture of the  $S = 0$   $Fe^{II}$  description into the ground state.

X-band EPR spectra taken at 4.2 K for microcrystalline samples of the  $I_3^-$ ,  $Br_2I^-$ , and  $I_2Br^-$  salts of the mixed-valence biferrocenium cation are shown in Figure 7. The *g* values evaluated from these and other EPR spectra are given in Table III. It is evident that the EPR spectra for the  $I_3^-$  and  $Br_2I^-$  salts are quite similar with

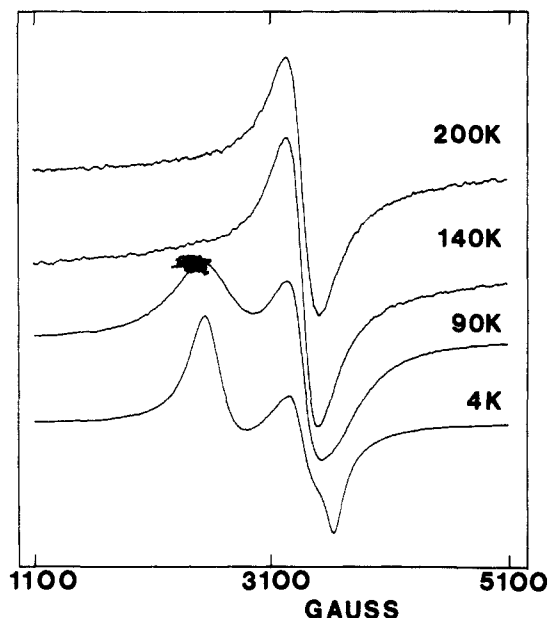


Figure 8. Variable-temperature X-band EPR spectra for a powdered sample of biferrocenium  $PF_6^-$ .

$\Delta g$  values of 1.93 and 1.85, respectively, at 4 K. The  $I_2Br^-$  salt also exhibits an axial EPR spectrum; however,  $\Delta g$  ( $=1.33$ ) is considerably reduced. There are significant conclusions that can be made on the basis of the spectrum for the  $I_2Br^-$  salt. First, it is clear that the  $I_2Br^-$  salt is not a mixture of  $I_3^-$  and  $Br_2I^-$  salts. Second, it is likely that neither does the  $I_2Br^-$  salt have a random distribution of  $I_3^-$ ,  $I_2Br^-$ ,  $Br_2I^-$ , etc., anions in one lattice nor is the  $I_2Br^-$  anion disordered in the crystals. Both of these situations would be expected to lead to more than one type of biferrocenium cation site in the lattice by virtue of different anion environments, and more than one EPR signal would have been expected. Support for the suggestion that the  $I_2Br^-$  anions are ordered in the lattice also can be seen in the fact that relatively intense peaks are evident in the powder X-ray diffraction pattern for this compound. There are only a few X-ray structures available for  $I_2Br^-$  salts. The  $I_2Br^-$  anions are ordered in  $CsI_2Br$ ,<sup>26</sup> whereas, they are disordered in the organic conductor  $\beta$ -(ET)<sub>2</sub> $I_2Br$ ,<sup>15</sup> where "ET" is bis(ethylenedithio)tetrathiafulvalene.

Since biferrocenium  $I_2Br^-$  is clearly isostructural with the  $I_3^-$  salt (vide supra), in the  $I_2Br^-$  salt there are stacks of biferrocenium cations surrounded by four stacks of  $I_2Br^-$  anions. Each mixed-valence cation has four neighboring  $I_2Br^-$  anions. If these four  $Br-I-I^-$  anions all have their bromine ends in the same direction, then it is conceivable that the biferrocenium cation in this salt would experience a greater low-symmetry crystal field than in the  $I_3^-$  and  $Br-I-Br^-$  salts. This could be the origin of the reduced  $\Delta g$  value.

A figure is available in the supplementary material to illustrate the temperature dependence of the EPR spectrum of biferrocenium  $Br_2I^-$ . As the temperature is increased above 4 K, the  $g_{\parallel}$  and  $g_{\perp}$  signals broaden such that above  $\sim 150$  K no EPR signal is seen. This type of behavior has been seen for other mixed-valence biferrocenes.<sup>5,8</sup>

The EPR characteristics of biferrocenium  $PF_6^-$  are both intriguing and puzzling. Variable-temperature spectra are presented in Figure 8, where it can be seen that at 4 K three features can be seen at *g* values of 2.65,  $\sim 2.01$ , and 1.86. An increase in the temperature leads to the broadening and disappearance of the 2.65 and 1.86 signals. At 140 K only a single "derivative-like" signal with  $g = 2.07$  remains. This signal basically remains unchanged up to 300 K ( $g = 2.02$ ). Double integration of the EPR signal from 4 to 300 K shows that the signal intensity has a Curie-like behavior. The spectral area is inversely proportional to the absolute temperature in the 4–300 K range as you would expect for a simple

(25) Duggan, D. M.; Hendrickson, D. N. *Inorg. Chem.* 1975, 14, 955.

(26) Carpenter, G. B. *Acta Crystallogr.* 1966, 20, 330.

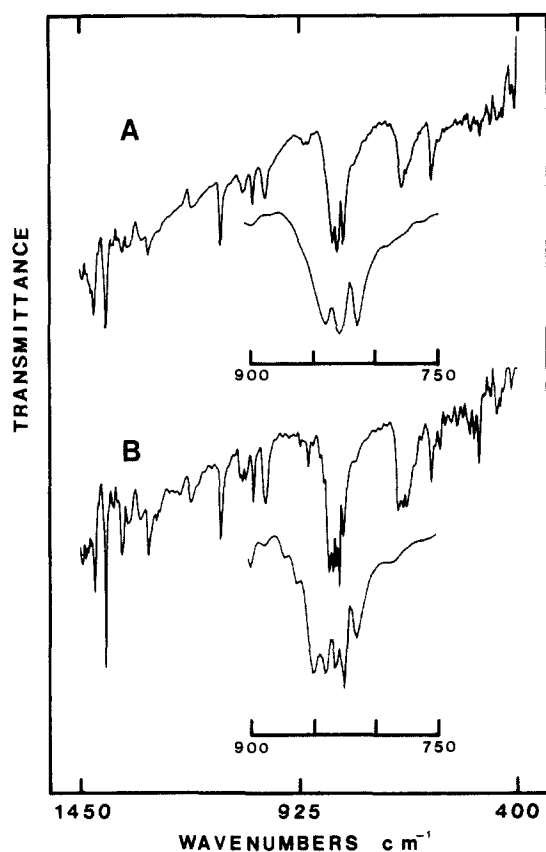


Figure 9. KBr-pellet FTIR spectra for biferrocenium  $I_2Br^-$  at two temperatures: 300 K (A); 50 K (B).

paramagnet. It is not clear what the origin of the  $g = 2.07$  signal is. It is interesting to note that the  $g$  value is close to the average ( $=2.12$ ) of the low-temperature  $g_{\parallel}$  and  $g_{\perp}$  signals. It does not seem that it is possible to assign the high-temperature  $g = 2.02$  signal to mixed-valence biferrocenium cations which are involved in intramolecular electron transfer at a rate that is in excess of what the EPR technique can sense for two reasons. First, such a species with a fast rate of intramolecular electron transfer is also expected to give an axial EPR signal, not a single derivative-like feature.<sup>5</sup> Second, the Mössbauer data indicate that at 300 K the intramolecular electron transfer rate is no faster than  $\sim 10^7$  s<sup>-1</sup>. It would require a rate of  $\sim 10^{10}$  s<sup>-1</sup> to "average" two EPR signals separated by  $\sim 100$  G.

The  $g = 2.02$  signal for biferrocenium  $PF_6^-$  at 300 K could be due to a magnetic exchange interaction between paramagnetic  $Fe^{III}$  ions in neighboring biferrocenium cations. If the intercation magnetic exchange interaction ( $\hat{H} = -2J\hat{S}_1\hat{S}_2$ ) increased with increasing temperature such that  $|J| > 0.01$  cm<sup>-1</sup> above  $\sim 200$  K, then the frequency ( $> 10^{10}$  s<sup>-1</sup>) of electron exchange between  $Fe^{III}$  ions would exceed the EPR time scale. Depending on the relative orientation of magnetic axes between  $Fe^{III}$  ions on neighboring sites, such a rapid exchange of electrons could give an "average"  $g$ -value signal. Further work is needed to understand the origin of the  $g = 2.02$  "average" signal.

**Infrared Spectroscopy.** As detailed in previous papers,<sup>4,5,27</sup> infrared spectroscopy has been employed to study mixed-valence biferrocenes. The perpendicular cyclopentadienyl C–H bending mode for a  $Fe^{II}$  metallocene typically occurs in a range from 805 to 815 cm<sup>-1</sup>. The corresponding band for a  $Fe^{III}$  metallocene is found in the range of 850 to 860 cm<sup>-1</sup>. Thus, a mixed-valence biferrocenium cation that has an appreciable potential energy barrier for intramolecular electron transfer and, consequently, does not have a completely delocalized electronic structure would be expected to show both  $Fe^{II}$  and  $Fe^{III}$  perpendicular C–H bending bands.

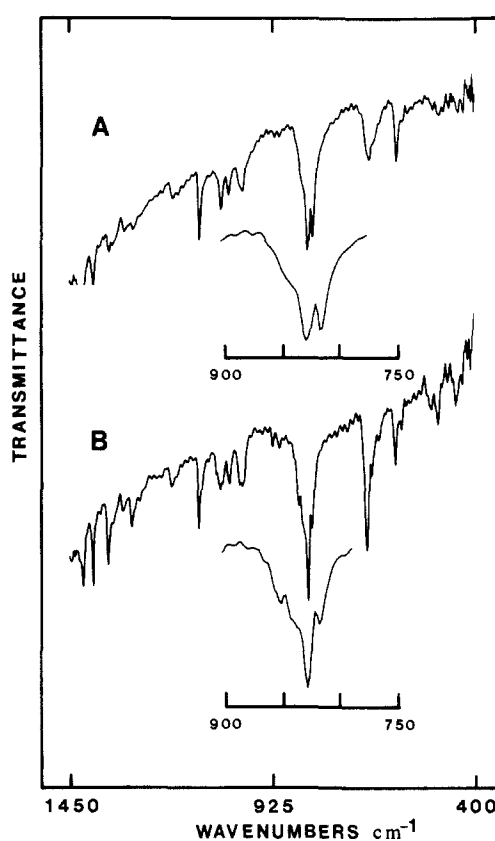


Figure 10. KBr-pellet FTIR spectra for biferrocenium  $Br_2I^-$  at two temperatures: 300 K (A); 50 K (B).

Variable-temperature (50–300 K) FTIR spectra were run for KBr pellets of the  $I_3^-$ ,  $I_2Br^-$ , and  $Br_2I^-$  salts of the biferrocenium cation. Unoxidized biferrocene shows two strong C–H bending bands at 812 and 820 cm<sup>-1</sup>. The spectra of the  $I_3^-$  and  $I_2Br^-$  biferrocenium salts look very similar in this region. Three bands at 816, 826 (with a shoulder at 833), and 840 cm<sup>-1</sup> are seen at 300 K, and four bands at 826, 833, 839, and 849 cm<sup>-1</sup> are seen at 50 K for biferrocenium  $I_3^-$ . In Figure 9 are given the 50 and 300 K spectra for the  $I_2Br^-$  salt (spectra for the  $I_3^-$  salt are available in the supplementary material). The  $I_2Br^-$  salt shows three bands at 816, 829, and 841 cm<sup>-1</sup> at 300 K and four bands at 816, 831, 841, and 849 cm<sup>-1</sup> at 50 K spectrum (see Figure 9). It is clear that the IR data for the  $I_3^-$  and  $I_2Br^-$  salts conclusively indicate the presence of  $Fe^{II}$  and  $Fe^{III}$  moieties in both cases.

As can be seen in Figure 10, at first glance the perpendicular C–H bending region for biferrocenium  $Br_2I^-$  looks somewhat different than for the other two trihalide salts. However, after careful comparison of the spectra it can be concluded that the  $Br_2I^-$  spectral pattern is related to the other two. It appears that certain bands have experienced small shifts which produce some overlapping of bands. At 50 K the  $Br_2I^-$  salt exhibits bands at 817 and 826 cm<sup>-1</sup> and a broad feature at 837 cm<sup>-1</sup>. It does appear to have  $Fe^{II}$  and  $Fe^{III}$  moieties.

**Micromodulation and the Electronic Localization–Delocalization Phase Transition.** There are at least three types of observations that indicate the presence of a phase transition, the nature of which controls the rate of intramolecular electron transfer in mixed-valence biferrocenes: (1) sample-history dependence of Mössbauer spectra which show signals from both localized and delocalized species; (2) the anion dependence of electron-transfer rate for the biferrocenium cation; and (3) endothermic peaks seen in heat capacity and DSC data for biferrocenium triiodide. The most dramatic case illustrating the first type of observation can be drawn from our work<sup>4</sup> on 1',6'-dibenzylbiferrocenium triiodide. A microcrystalline sample of this compound gives a 300 K Mössbauer spectrum which is dominantly that of a valence-localized species, i.e., one  $Fe^{II}$  and one  $Fe^{III}$  doublet. If the microcrystalline sample

(27) Kramer, J. A.; Hendrickson, D. N. *Inorg. Chem.* 1980, 19, 3330.

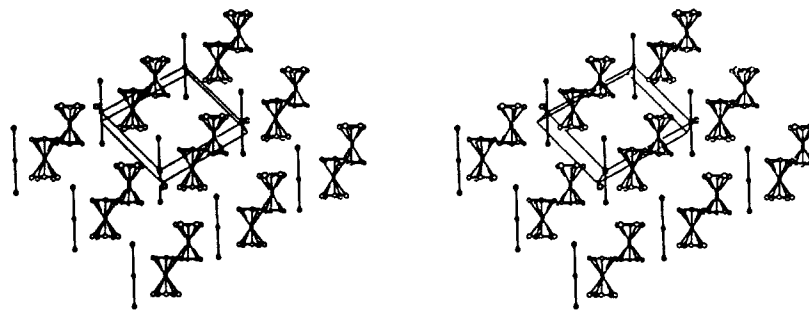


Figure 11. Stereoview of the packing arrangement in biferrrocenium triiodide.

is dissolved in  $\text{CH}_2\text{Cl}_2$  and hexane is allowed to diffuse into the  $\text{CH}_2\text{Cl}_2$  solution such that X-ray structure quality crystals grow, these crystals will give a 300 K Mössbauer spectrum which consists only of one average-valence doublet. The anion dependence of electron transfer in the case of the biferrrocenium cation was described above. Finally, the third type of observation has been thoroughly examined for biferrrocenium triiodide. This compound is now known<sup>4</sup> to convert from Mössbauer-localized at  $\sim 300$  K to Mössbauer-delocalized at  $\sim 357$  K. A DSC examination of several samples of biferrrocenium triiodide has revealed an endothermic peak in this temperature range. Furthermore, the heat capacity at constant pressure ( $C_p$ ) has been measured from 13 to 360 K for a 11-g sample of biferrrocenium triiodide.<sup>12</sup> At this time, it is only important to note that a sharp endothermic peak was seen at 328 K with two broader features at 312 and 346 K. A detailed analysis of these results will be presented later.<sup>12</sup>

A careful examination of Figure 11, which shows a stereoview of the packing arrangement in biferrrocenium triiodide, points to two *intermolecular* interactions that could be important in an electronic localization-delocalization phase transition. There are step-like stacks of biferrrocenium cations developing approximately along the  $\langle 011 \rangle$  direction. Cation-cation interactions develop as the result of the appreciable cyclopentadienyl-cyclopentadienyl contact between two cations. The Cp-Cp interplanar distance is only 3.4 Å. The second type of intermolecular interaction that could be important occurs between a mixed-valence cation and its nearest-neighbor anions. As mentioned above, each  $\text{I}_3^-$  ion is in essence a mixed-valence species. It can oscillate between two different forms, which in their limiting views can be represented as  $\text{I}_A-\text{I}_B\cdots\text{I}_C^-$  and  $\text{I}_A^-\cdots\text{I}_B-\text{I}_C$ . This oscillation in the inhomogeneous charge distribution in the neighboring  $\text{I}_3^-$  anions will impact on the rate of electron transfer in the mixed-valence cation.

It is appropriate to note that not only do the  $\text{I}_3^-$ ,  $\text{I}_2\text{Br}^-$ , and  $\text{Br}_2\text{I}^-$  salts of the biferrrocenium cation have the solid-state structure pictured in Figure 1 but also the 1',6'-di-X-substituted biferrrocenium triiodides where X can be ethyl, *n*-propyl,<sup>11</sup> or benzyl<sup>24</sup> are isostructural ( $P\bar{1}$  space group). Of course, from one compound to another the extent of Cp-Cp overlap between cations in the step-like stacks, as well as the magnitude of interaction between cation and neighboring anions, will change. In fact, from the X-ray structure<sup>4</sup> of 1',6'-di-*n*-butylbiferrrocenium triiodide ( $P2_1/C$  space group) it is clear that there is no Cp-Cp overlap between cations in this compound. The bulkiness of the *n*-butyl substituents has apparently led to the mixed-valence cations sliding away from each other. If this compound is to be viewed as consisting of step-like stacks of cations, then the interaction between cations is transmitted via one *n*-butyl group of one cation contacting the "top" of one cyclopentadienyl group of the next mixed-valence cation. However, this type of contact could still have the same effect as the Cp-Cp contact in determining the level of cooperativity in a given phase transition.

A qualitative description of the manner in which the above two intermolecular interactions lead to an electronic localization-delocalization phase transition can be given. First, consider the cation-cation interaction that develops down the step-like stack of mixed-valence cations. When an *intramolecular* electron transfer occurs in one cation, the two Cp rings bound to the  $\text{Fe}^{\text{II}}$  ion move away from the metal to assume the larger dimensions appropriate for a  $(\text{Cp})_2\text{Fe}^{\text{III}}$  moiety. At the same time the di-

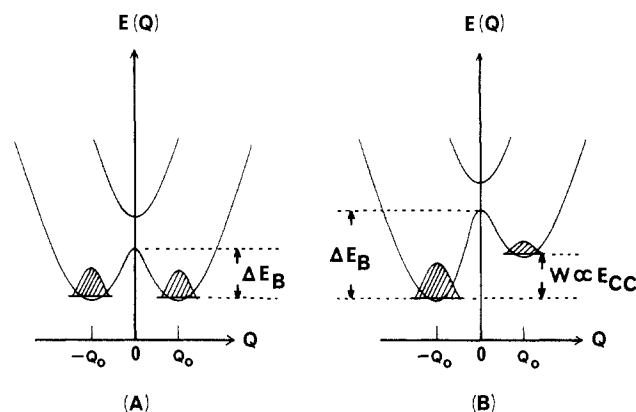
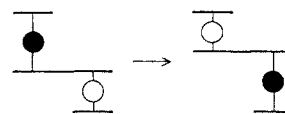


Figure 12. Potential energy plotted as a function of the out-of-phase combination of the two symmetric metal-ligand breathing vibrational modes on the two halves of a binuclear mixed-valence species. Diagram A is for a symmetric mixed-valence complex in the absence of environmental effects. Diagram B results if the environment about the binuclear mixed-valence complex is asymmetric.

mensions of the  $(\text{Cp})_2\text{Fe}^{\text{III}}$  moiety contract to those of a  $(\text{Cp})_2\text{Fe}^{\text{II}}$  species. The overall change can be represented schematically (overemphasized) as follows:



As detailed in the PKS vibronic model, a plot of the potential energy of such a mixed-valence complex as a function of this out-of-phase combination of Cp-Fe-Cp breathing modes ( $Q = Q_A - Q_B$ ) on the two halves of the biferrrocenium cation leads to the typical double-well potential energy diagram pictured in Figure 12A. Both the Coulomb interaction and the steric repulsion between two adjacent cations stabilize the state where each electron is localized on the equivalent iron ion in the two cations, that is, they stabilize the molecular distortion in the common direction as shown in Figure 13A. The cooperative electron localization or molecular distortion may be induced by the intercation interactions. Then, the stack of cations is in such an ordered localization or distortion state as indicated in Figure 13A: it has been found in 1',6'-di-*n*-propylbiferrrocenium triiodide<sup>11</sup> that ferrocene- and ferrocenium-like units are crystallographically discernible in the cation at 110 K. The potential energy curve for a cation becomes asymmetric in the ordered localization state as shown in Figure 12B. The energy difference  $W$  between the two potential wells for a single molecule is proportional to the cation-cation interaction,  $E_{CC}$ .<sup>28</sup> The potential energy barrier height for a single molecule is defined as  $\Delta E_B$  in Figure 12.

Three limiting cases develop for different relative values of  $\Delta E_B$  and  $E_{CC}$ . When  $\Delta E_B \gg E_{CC}$  and the  $\Delta E_B$  barrier is too high for a mixed-valence cation to transfer between the two potential wells, each stack of cations will remain fixed in an ordered arrangement at low temperature ( $k_B T < E_{CC}$ ) as indicated in Figure 13A. At

(28) Kambara, T.; Hendrickson, D. N.; Dong, T.-Y.; Cohn, M. J., publication in preparation.



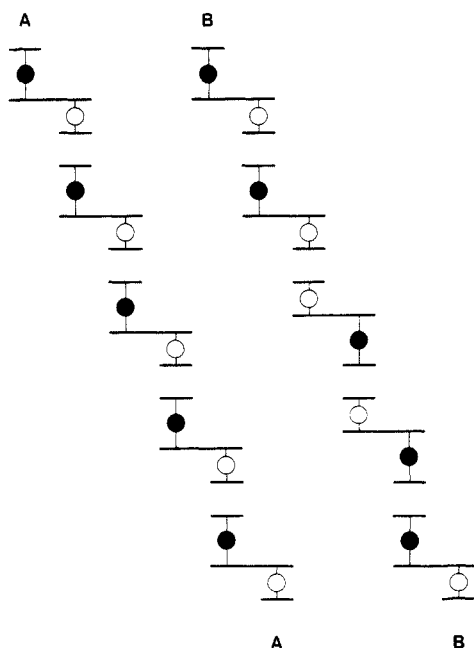


**Figure 13.** Schematic representations of different arrangements possible for a step-like stack of mixed-valence biferrocenium cations. Edgewise views of the cyclopentadiene and fulvalenide rings are shown. The  $\text{Fe}^{\text{II}}$  metallocene unit is indicated to have a smaller ring-to-ring distance than the  $\text{Fe}^{\text{III}}$  metallocene unit. Drawing A shows an ordered stack of electronically localized biferrocenium cations. Drawing B shows a disordered stack of localized biferrocenium cations.

the low temperature each cation occupies only the lower potential well in Figure 12B. As the temperature is increased, the thermal energy  $k_B T$  may exceed  $E_{CC}$  ( $\approx W$ ) and many cations may occupy the higher potential well. Then, the cooperative order of the electron localization in the stack of cations disappears and the potential energy curve becomes symmetric. The electronically localized molecules in the stack will become disordered as indicated schematically in Figure 13B.

If  $\Delta E_B$  and  $E_{CC}$  are of comparable magnitude, then certain mixed-valence cations in a stack can become activated and transfer an electron. Thermal energy is focused in a few mixed-valence cations as a result of the appreciable intermolecular interaction, and these few cations transfer an electron and adjust their molecular dimensions. It is possible that the activated cations will function as a soliton, that is, a boundary region between two domains which possess the opposite sense of valence localization. Regions (solitons) in the stack of cations will appear where cations have equal geometries on the two metallocene moieties. A schematic representation of a soliton between two localized domains is shown in Figure 14A. The soliton is comprised of a number of cations in various degrees of distortion intermediate between  $Q_0$  and  $-Q_0$  (see Figure 12). These solitons would be moving down (and up) the cation stacks at some characteristic velocity.

The dynamical equation for the soliton in a stack of mixed-valence biferrocenium cations<sup>28</sup> is qualitatively equivalent to the equations for ferroelectrics<sup>29</sup> and for polyacetylene,<sup>30</sup> but the detailed property of the soliton is different from the latter cases. When the temperature is increased and the thermal energy  $k_B T$  approaches to  $E_{CC}$  ( $\sim \Delta E_B$ ), rapid electron transfer may occur in a large fraction of the mixed-valence cations in the stack. The concentration of solitons has increased to the point that solitons are frequently moving past a given cation. Consequently, each cation is rapidly inverting between the two vibronic states. When the temperature exceeds  $E_{CC}/k_B$ , the order of electron localization in the stack disappears, that is, there is no domain. The electron in each cation is delocalized and every cation has

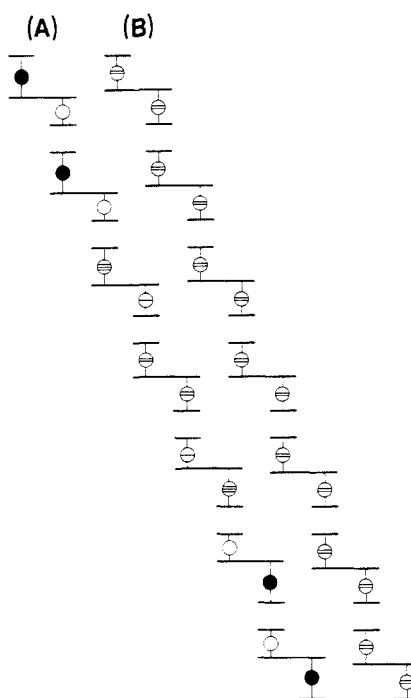
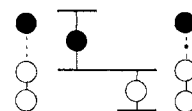


**Figure 14.** Drawing A shows a soliton between two ordered regions of electronically localized biferrocenium cations. Drawing B shows a stack of electronically delocalized biferrocenium cations.

equal geometry on the two metallocene moieties as indicated in Figure 14B.

In the third limiting case when  $\Delta E_B \ll E_{CC}$ , each stack is ordered at a low temperature of  $k_B T \ll E_{CC}$ , even though the thermal energy is such that an individual isolated molecule would be able to go over the barrier  $\Delta E_B$ . Since nonlinear energy arising from the double-well potential of an individual cation is quite small compared with the linear intercation interaction energy  $E_{CC}$ , there is no soliton in the present case. As the temperature is increased and the thermal energy  $k_B T$  exceeds  $E_{CC}$ , the order in electron localization disappears in the stack and the electron in each cation is completely delocalized as indicated in Figure 14B.

If there are only interactions between cations in one stack, there will not be a phase transition if the system is one dimensional. From the previous sections the dramatic effect of changing the anion upon the intramolecular electron-transfer rate has been clearly established. In biferrocenium triiodide<sup>4</sup> the shortest Fe-I distances between the iron ions and the terminal atoms of the  $\text{I}_3^-$  anion are 5.2–5.7 Å. It is very likely that asymmetry in charge distribution which develops in the triiodide anion will directly affect the potential energy diagram of the mixed-valence biferrocenium cation. Consider the positioning of two asymmetric  $\text{I}_3^-$  anions next to a biferrocenium cation, viz.:



If the shaded atom of the  $\text{I}_3^-$  is further from the central iodine atom and carries more negative charge than the other terminal iodine atom, there will be valence localization in the mixed-valence cation. The potential energy diagram of the mixed-valence cation is made to be asymmetric as indicated in Figure 12B. The Coulomb interaction with two anions which have such an asymmetric charge distribution will introduce a large zero-point energy difference between the two vibronic states of the mixed-valence cation. The ironic point is that the  $\text{I}_3^-$  anion could be a mixed-valence species as well. In the absence of any environmental effects, the  $\text{I}_3^-$  anion has a symmetric double-well potential energy diagram as in Figure 12A. If the cation environment about a  $\text{I}_3^-$  anion is not symmetric, the  $\text{I}_3^-$  anion will have an asymmetric potential energy diagram as in Figure 12B. It has been observed

(29) Krumhansl, J. A.; Schrieffer, J. R. *Phys. Rev. B* **1975**, *11*, 3535.

(30) Su, W. P.; Schrieffer, J. R.; Heeger, A. J. *Phys. Rev. B* **1980**, *22*, 2099.

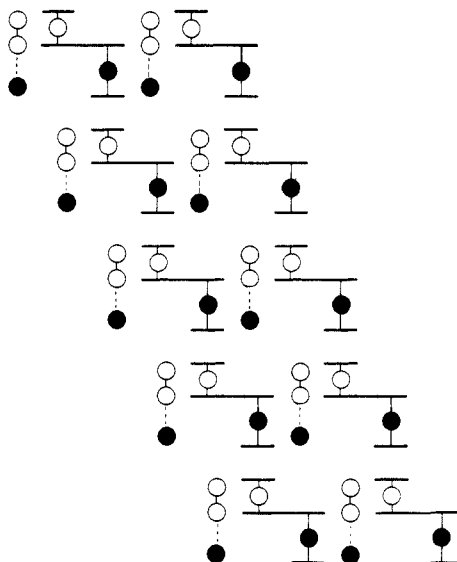


**Figure 15.** Schematic representation of a two-dimensionally-ordered section of biferrocenium triiodide.

in 1',6'-di-*n*-propylbiferrocenium triiodide<sup>11</sup> at 110 K that bond distances of I(1)–I(2) and I(1)–I(3) are different in each  $I_3^-$  anion.

With the type of cation–cation and cation–anion interactions described above, it is possible to understand why at low temperature there could be three-dimensional order in a crystallite of biferrocenium triiodide. A schematic representation of a two-dimensionally ordered section of biferrocenium triiodide is shown in Figure 15. The exact nature of a phase transition which will occur as the temperature of such an ordered phase is increased will depend on the relative magnitudes of the cation–cation and cation–anion interactions as well as other factors such as defect structure.

In the context of the above model it is understandable how the change from  $I_3^-$  to  $Br_2I^-$  for the counterion could lead to a change of  $\sim 150$  deg in the temperature at which the mixed-valence

biferrocenium cation transfers faster than the Mössbauer time scale. The Br–I bonding interaction in  $Br_2I^-$  is weaker than the I–I bonding interaction in  $I_3^-$ , and as a consequence  $\Delta E_B$  (Figure 12A) would be smaller for  $Br_2I^-$  than for  $I_3^-$ . Thus, the  $Br_2I^-$  anion would begin to oscillate between its two forms at lower temperatures than the  $I_3^-$  anion if the cation–anion interaction is greater than or comparable to the cation–cation interaction. This anion charge oscillation would lead to the onset of *intramolecular* electron transfer in the biferrocenium cation at a lower temperature for the  $Br_2I^-$  salt than for the  $I_3^-$  salt.

The sample-history dependence of the Mössbauer signals and DSC thermal effects seen for these mixed-valence biferrocenium salts are also explicable in terms of the above discussion. Crystalline samples prepared in different experiments can have appreciably different defect concentrations. Defects exist generally in profusion in crystalline material. There can be point defects such as vacancies or isolated impurities, line defects such as crystallographic dislocations, and a variety of surface defects. These defect sites serve as preferred sites of nucleation of critical size nuclei of a minority phase within a majority phase. The critical size nuclei grow at some rate eventually to become domains of the majority phase. If a minority-phase nucleus encounters defect structure as it is growing in size, the activation energy for further growth will be appreciably increased. It is understandable why the properties of a microcrystalline sample of a mixed-valence biferrocenium salt could be quite different from those of a more crystalline sample.

**Acknowledgment.** We are grateful for support from National Institutes of Health (Grant HL13652).

**Registry No.** Biferrocenium  $I_3^-$ , 39470-17-2; biferrocenium  $I_3Br^-$ , 102649-03-6; biferrocenium  $IBr_2^-$ , 99874-85-8; biferrocenium  $PF_6^-$ , 70282-49-4; biferrocene, 1287-38-3.

**Supplementary Material Available:** Figure 1, temperature dependence of X-band EPR spectrum for a powdered sample of biferrocenium  $Br_2I^-$ , and Figure 2, KBr pellet FTIR spectra for biferrocene and biferrocenium triiodide (2 pages). Ordering information is given in any current masthead page.